Journal of Power Sources 247 (2014) 858–864

Contents lists available at ScienceDirect

Journal of Power Sources

journal homepage: www.elsevier.com/locate/jpowsour

Short communication

Compositionally continuously graded cathode layers of $(Ba_{0.5}Sr_{0.5})(Fe_{0.91}Al_{0.09})O_{3-\delta}$–$Gd_{0.1}Ce_{0.9}O_2$ by wet powder spraying technique for solid oxide fuel cells

Taizhi Jiang, Zhenhua Wang*, Baiyu Ren, Jinshuo Qiao, Wang Sun, Kening Sun*

Beijing Key Laboratory for Chemical Power Source and Green Catalysis, School of Chemical Engineering and Environment, Beijing Institute of Technology, Beijing 100081, PR China

HIGHLIGHTS

- CGCLs were successfully fabricated by WPS technique.
- CGCLs exhibited continuously graded TEC between electrolyte and cathode.
- The components distribution visually proves the elaborate structure of CGCLs.
- Single cell of BSFA–GDC CGCLs reached the power density of 848 mW cm^{-2} at 800 °C.

ARTICLE INFO

Article history:
Received 6 July 2013
Received in revised form
4 September 2013
Accepted 7 September 2013
Available online 20 September 2013

Keywords:
Continuously graded cathode layers
Thermal expansion behavior
Wet powder spraying
Solid oxide fuel cells

ABSTRACT

Compositionally continuously graded cathode layers (CGCLs) of $(Ba_{0.5}Sr_{0.5})(Fe_{0.91}Al_{0.09})O_{3-\delta}$–$Gd_{0.1}Ce_{0.9}O_2$ (BSFA–GDC) have been constructed by a handy and effective technique called wet powder spraying (WPS). CGCLs exhibit similar thermal expansion coefficient (TEC) value between adjacent thin layers. The continuously graded structure and the well-distributed components of BSFA–GDC cathode are confirmed by morphological characterization with scanning electron microscopy (SEM), and by compositional analysis with energy dispersion X-ray spectrometer (EDS), respectively. The polarization resistance (R_p) of CGCLs with three different thicknesses is investigated by electrochemical impedance spectra (EIS). The EIS results show that CGCLs with a moderate thickness of 20 μm achieve the lowest R_p of 0.301 Ω cm^2 at 800 °C. In addition, anode-supported single cells with the configuration of NiO–YSZ/YSZ/GDC/BSFA–GDC have been fabricated and tested. The cell with the CGCLs thickness of 20 μm reaches the highest output power density of 848 mW cm^{-2} at 800 °C.

1. Introduction

Although Solid Oxide Fuel Cells (SOFCs) are attractive to researchers for recent decades because of their distinctive advantages including high energy-conversion efficiency, low environmental hazard, and excellent flexibility with various fuels [1], high operating temperature (800–1000 °C) which invites performance degradation and high cost severely impedes their commercial and industrial applications [2–4]. Many efforts have therefore been done focusing on the development of intermediate-temperature SOFCs (IT-SOFCs) whose operating temperature is between 600 °C and 800 °C [5–8]. During these works, optimizing the performance of the cathode is the most challenging task due to a sharp decline in the activity of the cathode when lowering temperature [8].

One approach to address this challenge is to meliorate the microstructure of the cathode [9,10]. Processing the cathode microstructure creates significant reduction on overall polarization of the cathode, and betters the cathode performance [10]. Among those processing parameters, enlarging the triple-phase boundary (TPB) is a publicly approved strategy, since it is generally recognized that most electrochemical reactions occur at TPB where electrons, oxygen ions, and oxygen gas coexist [11–13]. Besides the optimization on microstructure, developing new cathode materials of higher electrochemical performance is another feasible way to fabricate cathodes of IT-SOFCs [14,15]. Previously reported $(Ba_{0.5}Sr_{0.5})(Fe_{0.91}Al_{0.09})O_{3-\delta}$ (BSFA) exhibits high oxygen permeation [16] and acceptable electrochemical performance, which make it qualified to be a candidate for the

* Corresponding authors. Tel./fax: +86 (0)10 6891 8696.
E-mail addresses: dr.wangzhenhua@yahoo.com.cn (Z. Wang), bitkeningsun@yahoo.com.cn (K. Sun).

0378-7753/$ – see front matter © 2013 Elsevier B.V. All rights reserved.
http://dx.doi.org/10.1016/j.jpowsour.2013.09.034

cathode of SOFCs for the first time [15]. The success of BSFA is not accidental because aluminum-doped perovskite structure in B-site results in the diminution of nonstoichiometric oxygen variations and more stable redox behavior. Additionally, iron in this structure exhibits less flexible redox behavior and more stable high-spin state, which is beneficial to the long-term stability of the material [15].

However, during the operation of SOFCs, the residual stress caused by the discontinuity in thermal expansion coefficients (TECs) between adjacent materials is accumulated, which brings about the decay and even the failure of SOFCs [17]. This problem is especially serious with BSFA, because ferrite of perovskite structure possesses larger TEC [18]. Several strategies have been reported to deal with the problem. Composite cathode formed by mixing a second phase (usually the ionic conductive electrolyte materials) can reduce the difference in TEC between the cathode and the electrolyte [19–21]. More recently, functionally graded cathode comprised of three layers has been reported [17,22]. However, neither of these methods can solve the problem completely. Composite cathode has a limit mount of electrolyte material because excess electrolyte material will reduce the TPB sites and current conductivity [17]. Triple-layer graded cathode cannot utterly eliminate the mismatch among layers either [22]. Herein, a design of BSFA–GDC compositionally continuously graded cathode layers (CGCLs) have been proposed. If the multilayer cathode is compositionally and continuously graded, it can not only increase active sites of TPB [10], but can also match the TECs between the cathode and the electrolyte. Instead of an abrupt change between BSFA and GDC, CGCLs provide layers at which composition and microstructure gradually change from one material to the other [23,24].

To construct CGCLs, various techniques have been devised, such as electrophoretic co-deposition (EPD) technique, vacuum plasma spraying (VPS), flame spraying (FS), atmospheric plasma spraying, electron beam physical vapor deposition (EB-PVD), and ceramic ink jet printing [13,25–27]. However, these methods are either costly or complicate. In this paper, CGCLs combined with BSFA–GDC compositional cathode of superior electrochemical performance were prepared by a simple wet powder spraying (WPS) technique which is a non-contact versatile technique suitable for the coating of different shaped substrates with an adequate control of thickness [28–30]. Subsequently, microstructure, composition, and electrochemical performance of BSFA–GDC CGCLs and single cells with the construction of NiO–YSZ/YSZ/GDC/BSFA–GDC are characterized.

2. Experimental

2.1. Preparation of powders

$(Ba_{0.5}Sr_{0.5})(Fe_{0.91}Al_{0.09})O_{3-\delta}$ (BSFA) powders were synthesized by a combined citric acid and ethylene-diamine-tetraacetic acid (EDTA) method. Given amounts of $Ba(NO_3)_2$, $Al(NO_3)_3$, $Fe(NO_3)_3$, and $Sr(NO_3)_2$ (all reagents are A.R.) were dissolved in deionized water, followed by addition of EDTA acid and citric acid with the controlled molar ratio of EDTA acid to citric acid to total metal cations at around 1:1.5:1. After agitation for certain time, the pH value of the solution was adjusted to approximately 9.0 by adding ammonia. The solution was put in a loft drier at 150 °C for 24 h. Then further heat treatments were applied, i.e., the precalcination for 2 h at 700 °C and the final calcination to obtain the pure perovskite phase for 10 h at 950 °C. $(Y_2O_3)_{0.08}(ZrO_2)_{0.92}$ (YSZ) and $Gd_{0.1}Ce_{0.9}O_2$ (GDC) powders were purchased from Tosoh Co., Japan and Fuel Cell Materials Inc., USA, respectively.

2.2. Process of WPS

The suspension for WPS deposition was prepared as below. BSFA and GDC powder, triethanolamine, polyvinyl butyral, and starch were mixed in ethanol and agitated with a rotational speed of 120 rpm for 24 h. Then the suspension was sprayed onto the substrate under the drive of carrier gas of air using a modified spraying gun (BD-128, Fenghua Bida Machinery Manufacture Co. Ltd., China) with the nozzle size of 0.35 mm (pore diameter). CGCLs were sprayed with gradually changing compositions of suspension, i.e. by gradually feeding BSFA suspension to GDC suspension drop by drop at a constant rate. The schematic diagram to construct CGCLs by WPS is illustrated in Fig. 1. After the spray deposition, BSFA–GDC CGCLs were calcinated at 1050 °C for 3 h in air.

2.3. Characterization

The phase and crystallinity of the BSFA powders, GDC powders and BSFA–GDC compositional cathode powders were examined by X-ray diffraction (XRD) analysis on Rigaku D/max-2000 X-ray diffractometer with monochromatic Cu Kα radiation (45 kV, 50 mA). Surface and cross-sectional fracture microstructure of the cathode were determined by scanning electron microscopy (FEI, QUANTA-250) equipped with an energy dispersion X-ray spectrometer (EDS).

For the thermal expansion coefficient (TEC) measurements, six powders, including YSZ, GDC, BSFA, BSFA–GDC (25:75 wt.%), BSFA–GDC (50:50 wt.%), and BSFA–GDC (75:25 wt.%) were prepared. Then each powder was uniaxially pressed into a bar-shaped die under a pressure of 500 MPa. After each bar was sintered at a certain temperature, the TEC of different material could be determined by a dilatometer (Netsch DIL 402C/4) over the 40 °C–1000 °C temperature range.

To investigate the cathode polarization resistance (R_p), a three-electrode was prepared. After CGCLs were fabricated by WPS on dense YSZ pellet which is prepared by dry-pressing method before sintering at 1500 °C for 5 h, platinum paste (Sino-Platinum Metals Co., China) was applied to the other side of YSZ pellet in symmetric configuration as the counter electrode (CE) and to the edge of the same side of electrolyte as reference electrode (RE). The Pt paste was calcined at 850 °C for 30 min. Then electrochemical impedance spectroscopy (EIS) was conducted over the temperature range of 650–800 °C using a potentiostat–galvanostat (PARSTAT M2273, Princeton Applied Research). The frequency range applied was from 10 mHz to 100 kHz with a signal amplitude of 5 mV.

Anode-supported single cells with the structure of NiO–YSZ/YSZ/GDC/BSFA–GDC were constructed before characterization. Ni/YSZ anode and YSZ electrolyte film were prepared by co-tape casting technology followed by sintering at 1400 °C. Then GDC interlayer and BSFA–GDC CGCLs were fabricated by WPS. *I–V* characteristics measurements were carried out with a Fuel Cell Test System (FCTS) produced by Arbin Instruments, with the cathode exposed to ambient air and the anode exposed to humidified (3 vol.% H_2O) hydrogen at a flow rate of 50 mL min^{-1}.

3. Results and discussion

3.1. X-ray diffraction analysis of cathode powders

X-ray diffraction (XRD) patterns of several powders are shown in Fig. 2. Fig. 2(a) and (b) demonstrates that the pattern of GDC powders corresponds to the fluorite structure and that the as-synthesized BSFA powders are highly phase-pure perovskite. We can also see from Fig. 2(c), (d), and (e) that BSFA–GDC composite cathode powders actually consist of two crystallized phases,

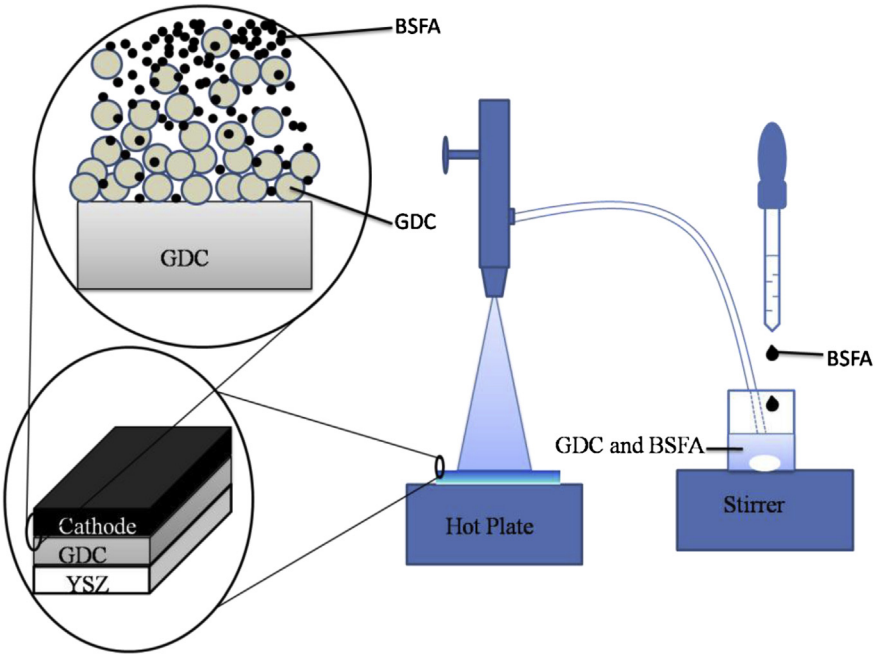

Fig. 1. Schematic diagram of spraying the CGCLs by WPS.

perovskite phase of BSFA and fluorite phase of GDC. Fig. 2(e) shows some small peaks (41° and 51°), which means BSFA reacts slightly with GDC to form insulator phase, such as $GdBa_2Fe_3O_{8.17}$, Al_8CeFe_4, and Fe_3Gd, at 1100 °C. This reaction will probably lead to degradation of cathode performance. Fig. 2(d) and (c) proves the small impurity peaks disappear when temperature decreases to 1050 °C or 1000 °C. Therefore, a reduced sintering temperature of 1050 °C is adequate in the following experiment to investigate CGCLs of BSFA–GDC.

3.2. Thermal expansion behavior of CGCLs

When fabricating fuel cells, the thermal expansion coefficients (TECs) of electrode and electrolyte should be taken into account because the mismatch of TECs will result in thermal stresses, residual stresses, and following degradation of fuel cells. In this experiment, the TEC of YSZ is 10.58×10^{-6} K^{-1}, while the TEC of BSFA is 27.28×10^{-6} K^{-1}. This severe mismatch of TECs will inevitably impair the longevity of SOFCs. According to our previous experiments, BSFA reacts with YSZ at high temperature, while GDC exhibits quite stable characteristic when attached to both YSZ and CCGLs. Moreover, the TEC of GDC interlayer (12.23×10^{-6} K^{-1}) is close to that of YSZ. Thus, instead of attaching BSFA to YSZ directly, a GDC interlayer has been inserted between cathode and electrolyte. Besides inserting an interlayer, compositionally continuously graded cathode layers (CGCLs) were proposed and prepared to avoid this sudden transition.

As shown in Figs. 3 and 4, pure BSFA possesses a high value of TEC and its dL/L_0 curve presents an inflection point at 400 °C. As a

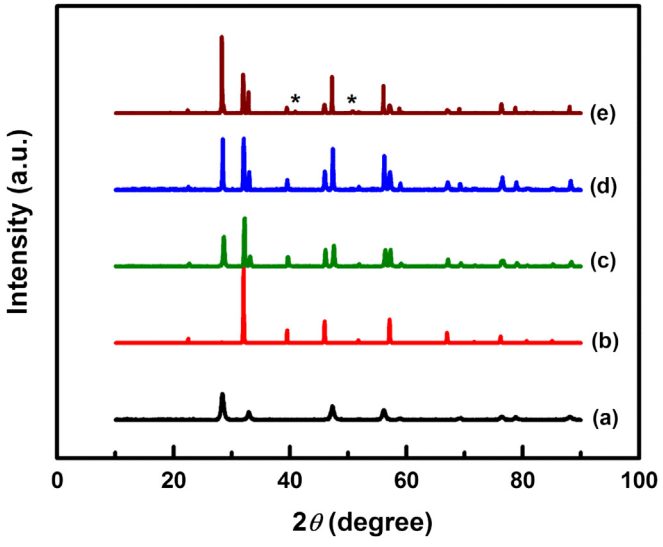

Fig. 2. X-ray diffraction patterns of GDC powders (a); BSFA powders (b); BSFA–GDC composition powders sintered for 3 h at the temperature of 1000 °C (c); 1050 °C (d); 1100 °C (e).

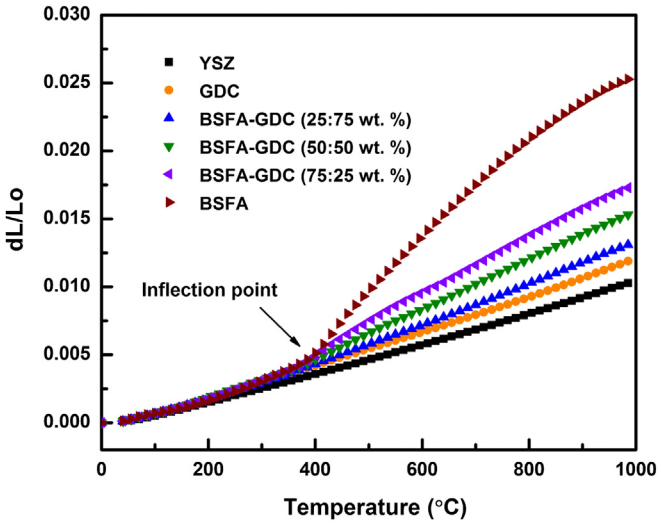

Fig. 3. Thermal expansion behavior of YSZ pellet, GDC interlayer, and CGCLs with different composition ratios.

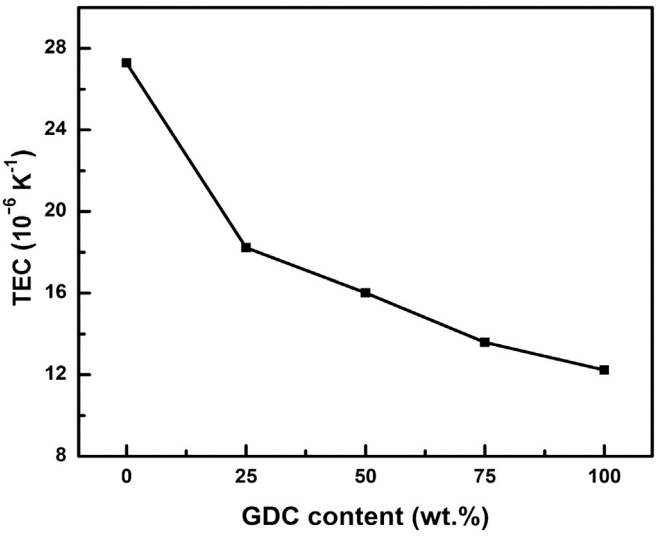

Fig. 4. Thermal expansion coefficient as a function of proportion of GDC in CGCLs.

result of the inflection point, the shrinkage rate, namely the TEC, increases from 13.94 × 10^{-6} K^{-1} to 33.41 × 10^{-6} K^{-1}. This change can be explained by lattice expansion due to the reduction of cations [18]. The loss of lattice oxygen caused by high temperature requires thermal reduction of B-site Fe^{4+} to Fe^{3+} to maintain the charge neutrality.

In this experiment, CGCLs were constructed to match the TECs between BSFA and GDC. The GDC content gradually increases in the CGCLs, from the cathode edge to the electrolyte. And the TEC of every thin layer decreases gradually with the increasing of GDC content, as shown in Fig. 3. This tendency is also shown in Fig. 4. Dramatically, when a small amount of GDC (25 wt.%) is blended in BSFA, the TEC drops from 27.28 × 10^{-6} K^{-1} to 18.22 × 10^{-6} K^{-1}. With further increase of GDC proportion in BSFA–GDC composition (50 wt.% and 75 wt.%), the TEC of BSFA–GDC composite is gradually approaching that of GDC. Thus, the TEC of every adjacent thin layer is practically identical along the compositional gradient, which indicates continuous gradation has been constructed and that delamination could be avoided by introducing CGCLs in SOFC.

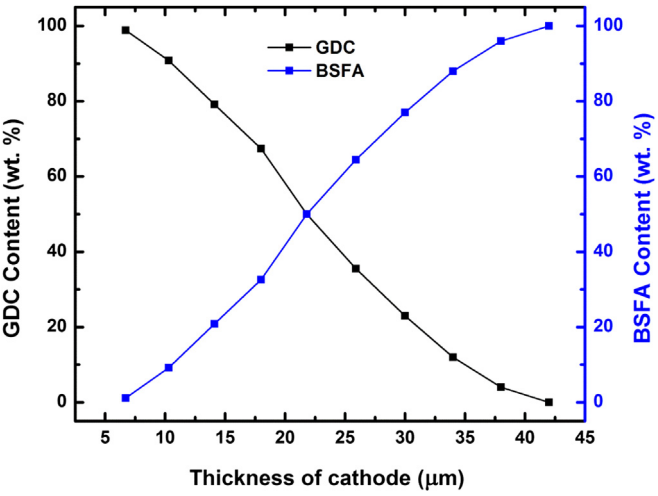

Fig. 5. The relationship between the composition of the BSFA–GDC CGCLs and the thickness.

3.3. Microstructural and compositional analysis of CGCLs

WPS is an effective way to construct CGCLs because the compositional gradient of CGCL can be readily controlled by adjusting the spraying rate (R_1) and the increasing rate (R_2) of concentration of BSFA in BSFA–GDC suspension. Within the same spraying time, if we control R_1 to a constant and increase R_2, the compositional gradient of CGCL will increase. Therefore, we can devise and construct a set of CGCLs with different compositional gradient.

In WPS suspension, the theoretical weight content of BSFA and GDC at any time can be obtained from the following Equations (1) and (2).

$$\frac{dW_{BSFA}}{dt} = R_2 C_{BSFA} - R_1 \times \frac{W_{BSFA}}{V_0 + (R_2 - R_1)t} \quad (1)$$

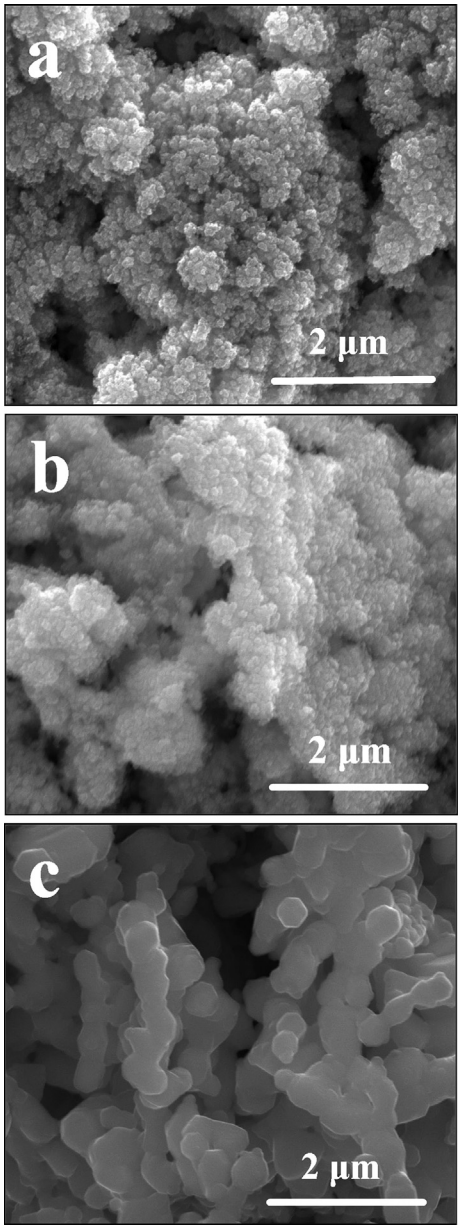

Fig. 6. Surface microstructure of BSFA–GDC CGCLs after sintering at 1050 °C for 3 h at the thickness of 6 μm (a), 18 μm (b), and 30.00 μm (c).

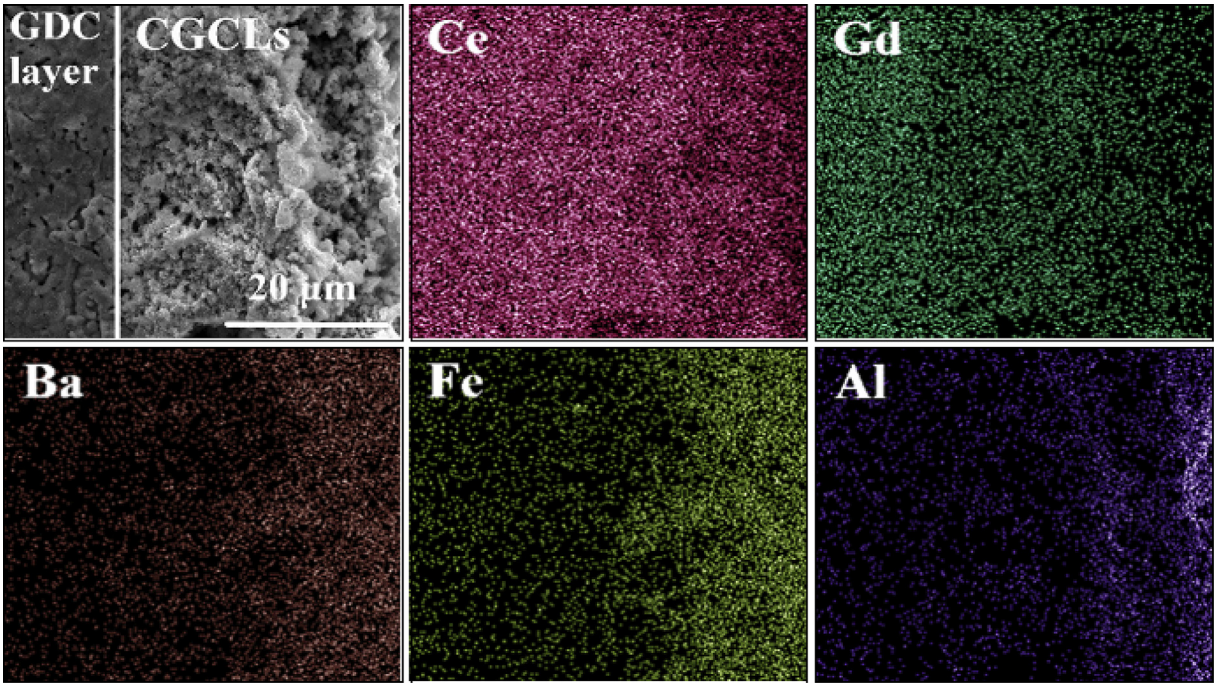

Fig. 7. Cross-sectional fracture micrograph and EDS dot mapping of CGCLs fabricated by WPS.

$$\frac{dW_{GDC}}{dt} = R_1 \times \frac{W_{GDC}}{V_0 + (R_2 - R_1)t} \quad (2)$$

In the equations above, when the spraying time is t, W_{BSFA} and W_{GDC} are the weight content of BSFA and GDC in WPS suspension, respectively. The constant value of C_{BSFA} is the concentration of BSFA suspension which is going to be feeded in GDC suspension. V_0 is the original volume of WPS suspension. And the proportion of BSFA, P_{BSFA}, at any time can be calculated by Equation (3).

$$P_{BSFA} = \frac{W_{BSFA}}{W_{BSFA} + W_{GDC}} \quad (3)$$

In this paper, R_1 and R_2 are both constant, thus, the compositional gradient is fixed and every thickness corresponds to a certain weight ratio of BSFA in CGCLs. The surficial weight ratios of BSFA and GDC in CGCLs with different thickness are easily calculated through the content of Fe and Ce element based on the EDS quantification results. Thus the relationship between the compositional content and CGCLs thickness is obtained, as shown in Fig. 5. Within the thickness of 42 μm, BSFA gradually replaces GDC.

Fig. 6 reveals the SEM surface images of CGCLs at the thickness of 6 μm (Fig. 6(a)), 18 μm (Fig. 6(b)), and 30 μm (Fig. 6(c)), where the surficial percentage of BSFA in CGCLs is 1 wt.%, 33 wt.%, and 77 wt.%, respectively. All the samples exhibit porous and uniform microstructures. With the thickening of CGCLs, the content of BSFA increases. As we can observe from Figs. 5 and 6, not only is the composition graded, but also the microscopic morphology differs

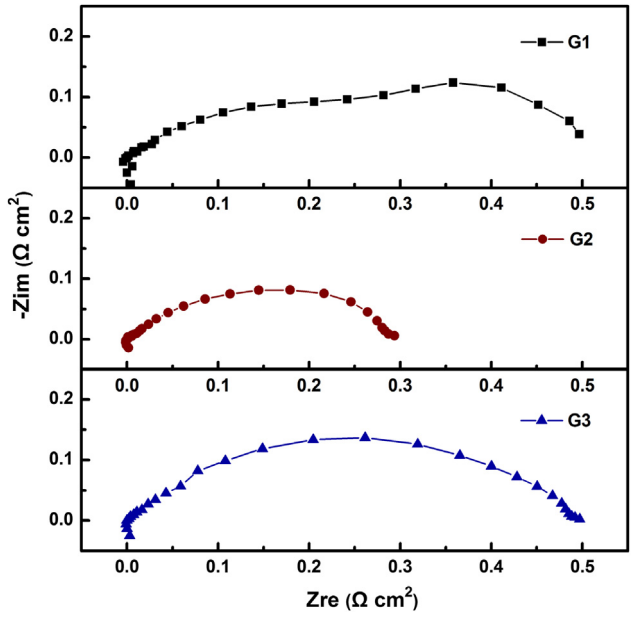

Fig. 8. The electrochemical impedance spectra of G1, G2 and G3 at 800 °C.

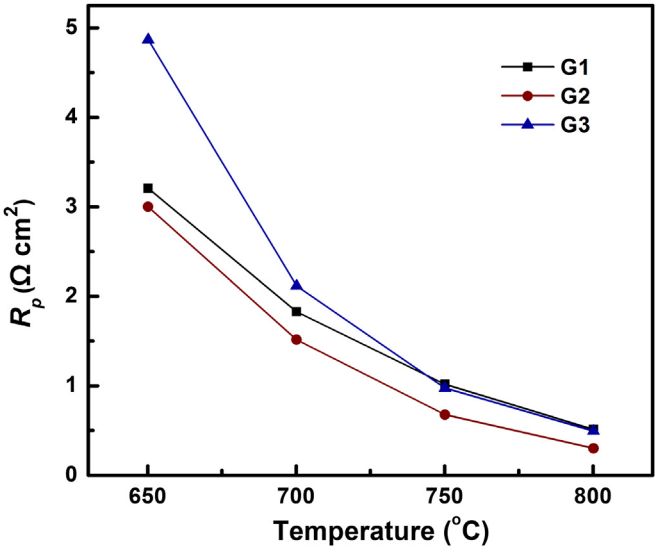

Fig. 9. Polarization resistance of G1, G2, and G3 as a function of temperature.

apparently. CGCLs with the thickness of 6 μm contain nanosized particles without aggregation. When the thickness increases to 18 μm, large particles appear with nanosized particles adhere to their surface. It is usually recognized that electrochemical reactions occur within the thickness between 0 and 20 μm [10]. Since CGCLs are constructed with elaborate architecture at this range, it is effective to increase specific surface area and the length of TPB, which is meaningful for the improvement of electrochemical performance of the cathode. Further thickening of CGCLs to 30 μm leads to aggregation of small particles, which is precipitated by high concentration of BSFA. A porous network of CGCLs is shown in Fig. 6(c), which ensures gas transport and current collection.

Fig. 7 reports the cross-sectional fracture micrograph of the CGCLs with the thickness of 26 μm where the surficial percentage of BSFA is from 0 to 65 wt.%. With the assist of EDS dot mapping technique, the compositional changes are explicit on the cross-sectional micrograph. As we can see in Fig. 7, within the range of 26 μm, the content of Ce and Gd gradually decreases from the GDC/BSFA–GDC interface to BSFA–GDC edge, while the content of Ba, Fe, and Al presents an opposite trend. No abrupt compositional transition is detected between adjacent layers. The EDS maps also imply CGCLs have been well constructed and delamination could be avoided because of the increased physical resilience.

3.4. Electrochemical analysis of EIS and I–V curves

Three CGCLs (noted as G1, G2, and G3) with the thickness of 13 μm, 20 μm, and 42 μm, respectively, were fabricated to investigate their electrochemical properties. The thickness selected is based on the proportion of BSFA. For the three thicknesses, the surficial proportion of BSFA is 21%, 50%, 99%, respectively. The electrochemical impedance spectra (EIS) of G1, G2, and G3 are performed at the temperature range of 650–800 °C. Fig. 8 shows the Nyquist plots of G1, G2, and G3 cathode on GDC/YSZ pellet measured at 800 °C in air. Each impedance plot is comprised of several arcs, and every arc corresponds to an electrochemical or a physical process. The intercept with real axis in high-frequency region represents the inherent ohmic resistance. The difference between the intercepts with real axis in high-frequency and low-frequency represents the polarization resistance (R_p), including the charge-transfer processes (the electron-transfer and ion-transfer processes occurring at the current collector/cathode and the cathode/electrolyte interfaces, respectively) and the diffusion processes (adsorption–desorption of oxygen, oxygen diffusion at the gas/cathode interface, and surface diffusion of intermediate oxygen species) [31,32]. In this experiment, the cathode polarization resistance (R_p) of G1, G2, and G3 at 800 °C is 0.513 Ω cm^2, 0.301 Ω cm^2, and 0.494 Ω cm^2, respectively. As we can see, with the increase of thickness of CGCLs, the R_p value initially decreases, and then increases. This is because the surficial BSFA content is relatively low (21%) at the thickness of 13 μm, which is not enough to catalyze the cathodic reaction completely. Moreover, this thickness is below the normal value of cathode thickness, which also implies an incomplete reaction at CGCLs. When the thickness increases to 20 μm, the minimum R_p value is obtained indicating that CGCLs facilitate the electron-transfer, O^{2-}-transfer, and O_2 diffusion processes. However, if the thickness reaches 42 μm, the path of O_2, O^{2-} and electron transport will be elongated, leading to the increase of R_p value.

The R_p values in air as a function of temperature for G1, G2, and G3 cathode are shown in Fig. 9. G2 possesses lowest R_p at all corresponding temperatures as a result of the optimal thickness. The R_p value of three CGCLs decreases from 650 °C to 800 °C. This is associated with an increase in ionic conductivity of GDC as the temperature increases.

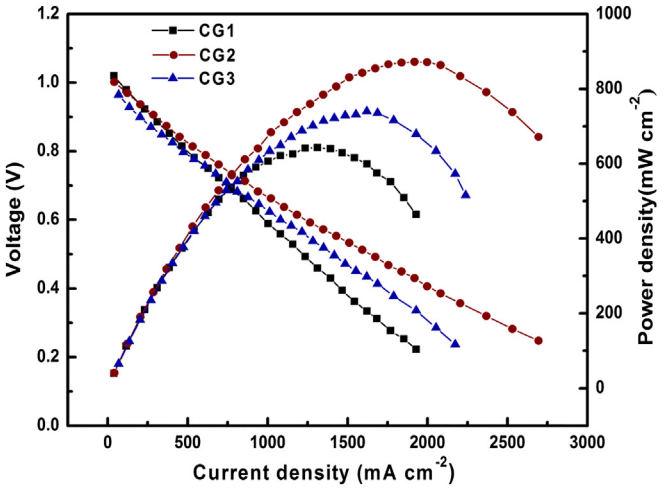

Fig. 10. Cell voltages and power densities as functions of current densities for CG1, CG2, and CG3 at 800 °C.

Electrochemical performance of the three SOFCs with CGCLs of G1, G2, and G3 is shown in Fig. 10. Similarly, the full cells are noted as CG1, CG2, and CG3, respectively. The observed peak power densities of CG1, CG2 and CG3 are about 632.92 mW cm^{-2}, 848.25 mW cm^{-2}, 737.06 mW cm^{-2} at 800 °C, respectively. The open circuit voltages (OCVs) are 1.045 V, 1.025 V, and 1.015 V for three SOFCs respectively. Both cathode polarization resistance and peak power density suggest that single cell with the CGCLs thickness of 20 μm on GDC/YSZ electrolyte has the best electrochemical performance among the three, which is in accordance with EIS analyzation above that excess or inadequate thickening of CGCLs will both lower the cell's performance.

4. Conclusions

In this paper, an optimized microstructure, continuously graded cathode layers (CGCLs), has been constructed by wet powder spray (WPS) technique to enhance the cathode performance of SOFC. BSFA–GDC continuously graded cathode layers (CGCLs) proved to be effective for preventing sudden change of TEC between the cathode and the electrolyte. In addition, BSFA as a novel material of high electrochemical performance has been applied to this well-graded framework. During this work, thickness of CGCLs was investigated. Three CGCLs with different thicknesses (13 μm, 20 μm, and 42 μm, respectively) were prepared and characterized. The EIS data showed that the lowest cathode polarization resistances (R_p) was 0.301 Ω cm^2 at 800 °C with a thickness of 20 μm. Meanwhile, the highest peak power density of 848.25 mW cm^{-2} was achieved at 800 °C with the same thickness.

Acknowledgments

This work was supported by the National Natural Science Foundation of China under contract No. 21076023 and No. 21006006, and also supported by the Foundation of Beijing Key Laboratory for Chemical Power Source and Green Catalysis under contract No. 2013CX02031.

References

[1] B.C.H. Steele, A. Heinzel, Nature 414 (2001) 345–352.
[2] R.A. George, N.F. Bessette, J. Power Sources 71 (1998) 131–137.
[3] K.J. Yoon, G. Ye, S. Gopalan, U.B. Pal, J. Fuel Cell Sci. 7 (2010) 021010-1–021010-5.

[4] B. Godfrey, K. Foger, R. Gillespie, R. Bolden, S.P.S. Badwal, J. Power Sources 86 (2000) 68–73.
[5] D. Pergolesi, E. Fabbri, A. D'Epifanio, E. Di Bartolomeo, A. Tebano, S. Sanna, S. Licoccia, G. Balestrino, E. Traversa, Nat. Mater. 9 (2010) 846–852.
[6] A. Esquirol, N.P. Brandon, J.A. Kilner, M. Mogensen, J. Electrochem. Soc. 151 (2004) A1847–A1855.
[7] S.W. Tao, J.T.S. Irvine, Adv. Mater. 18 (2006) 1581.
[8] E. Fabbri, L. Bi, D. Pergolesi, E. Traversa, Adv. Mater. 24 (2012) 195–208.
[9] Y. Liu, S.W. Zha, M.L. Liu, Chem. Mater. 16 (2004) 3502–3506.
[10] J. McCoppin, D. Young, T. Reitz, A. Maleszewski, S. Mukhopadhyay, J. Power Sources 196 (2011) 3761–3765.
[11] C.H. Li, S.H. Hu, K.W. Tay, Y.P. Fu, Ceram. Int. 38 (2012) 1557–1562.
[12] J.J. Choi, S.H. Oh, H.S. Noh, H.R. Kim, J.W. Son, D.S. Park, J.H. Choi, J. Ryu, B.D. Hahn, W.H. Yoon, H.W. Lee, J. Alloys Compd. 509 (2011) 2627–2630.
[13] W.S. Xia, H.O. Zhang, G.L. Wang, Y.Z. Yang, Adv. Eng. Mater. 11 (2009) 111–116.
[14] W. Zhou, J. Sunarso, J. Motuzas, F. Liang, Z. Chen, L. Ge, S. Liu, A. Julbe, Z. Zhu, Chem. Mater. 23 (2011) 1618–1624.
[15] Z. Lou, J. Qiao, Y. Yan, J. Peng, Z. Wang, T. Jiang, K. Sun, Int. J. Hydrogen Energy 37 (2012) 11345–11350.
[16] J. Martynczuk, F. Liang, M. Arnold, V. Sepelak, A. Feldhoff, Chem. Mater. 21 (2009) 1586–1594.
[17] C. Yang, Q. Xu, J. Power Sources 212 (2012) 186–191.
[18] Q. Zhou, L. Xu, Y. Guo, D. Jia, Y. Li, W.C.J. Wei, Int. J. Hydrogen Energy 37 (2012) 11963–11968.
[19] M.Z. Zheng, X.M. Liu, W.H. Su, J. Alloys Compd. 395 (2005) 300–303.
[20] S.Z. Wang, Y.M. Zou, Electrochem. Commun. 8 (2006) 927–931.
[21] X. Zhang, M. Robertson, S. Yick, C. Deces-Petit, E. Styles, W. Qu, Y. Xie, R. Hui, J. Roller, O. Kesler, R. Maric, D. Ghosh, J. Power Sources 160 (2006) 1211–1216.
[22] X. Ding, X. Kong, J. Jiang, C. Cui, L. Guo, Int. J. Hydrogen Energy 35 (2010) 1742–1748.
[23] N.T. Hart, N.P. Brandon, M.J. Day, N. Lapena-Rey, J. Power Sources 106 (2002) 42–50.
[24] C.R. Xia, W. Rauch, W. Wellborn, M.L. Liu, Electrochem. Solid-State Lett. 5 (2002) A217–A220.
[25] Z. Wang, N. Zhang, J. Qiao, K. Sun, P. Xu, Electrochem. Commun. 11 (2009) 1120–1123.
[26] M. Mott, J.R.G. Evans, Mater. Sci. Eng. A 271 (1999) 344–352.
[27] B. Meng, Y. Sun, X.D. He, M.W. Li, Mater. Sci. Technol. 24 (2008) 997–1001.
[28] E. Schuller, R. Vassen, D. Stover, Adv. Eng. Mater. 4 (2002) 659–662.
[29] W. Zhou, H. Shi, R. Ran, R. Cai, Z. Shao, W. Jin, J. Power Sources 184 (2008) 229–237.
[30] N. Oishi, Y. Yoo, I. Davidson, J. Am. Ceram. Soc. 90 (2007) 1365–1369.
[31] W. Zhou, R. Ran, Z. Shao, R. Cai, W. Jin, N. Xu, J. Ahn, Electrochim. Acta 53 (2008) 4370–4380.
[32] M.J. Jorgensen, M. Mogensen, J. Electrochem. Soc. 148 (2001) A433–A442.